# The concentration of bone-related organic additives drives the pathway of apatite formation

Marc Robin, Camila B Tovani, Jean-Marc Krafft, Guylène Costentin, Thierry Azaïs, Nadine Nassif

HAL Id: hal-03335945

https://hal.sorbonne-universite.fr/hal-03335945v1

Submitted on 6 Sep 2021

# The concentration of bone-related organic additives drives the pathway of apatite formation

*Marc Robin[1][§], Camila B. Tovani[1][§], Jean-Marc Krafft[2], Guylène Costentin[2]\*, Thierry Azaïs[1],*

*Nadine Nassif[1] \**

*1. Sorbonne Université, CNRS, Collège de France, Laboratoire Chimie de la Matière Condensée*

*de Paris, LCMCP, F-75005 Paris, France.*

*2. Sorbonne Université, CNRS, Laboratoire Réactivité de Surface, LRS, F-75005 Paris, France.*

*[§] These authors contributed equally to this work*

*\*Corresponding author e-mail:*

*guylene.costentin@sorbonne-universite.fr, nadine.nassif@sorbonne-universite.fr*

**Keywords: biomineralization, calcium phosphate, additives, biopolymers, confinement**

**Abstract**

Bone models set for studying apatite mineralization tend to use excess of organic additives and a very low concentration of collagen in the light of those described in the biological tissue. However, the activity of soluble additives during mineral deposition is highly dependent on their concentration and confinement state, among others. Here, we investigate the role of concentration of organic additives described as key components in bone mineralization, *i.e.* the bioinspired synthetic polyaspartate mimicking non-collagenous protein (NCP), citrate and collagen, on apatite formation. The precipitation set-up tends to mimic the acidic mineralization front in bone and was monitored by *in situ* Raman and *ex situ* solid-state nuclear magnetic resonance (ssNMR). This model helps to identify specific effects of organic additives on mineral formation. In particular, we show that the sequence of apatite precursors often described *in vitro*, *i.e.* amorphous calcium phosphate (ACP) and subsequent octacalciumphosphate (OCP) formation, is noticeably modified by varying the concentration of the additives. NCP and citrate are identified as either inhibitor or activator in the formation of calcium phosphate (CaP). Besides, collagen acts either as additives or as organic scaffold below and above the liquid-crystal threshold, respectively. This result highlights that confinement drives thermodynamically apatite formation by slowing down the kinetic formation of precursors, even at alkaline pH.

# 1. INTRODUCTION

Biomineralization is a multistep process whereby organisms create fascinating multifunctional hybrid structures displaying hierarchical organization and well-defined crystal size, morphology, spatial orientation and polymorphs selection.[1] The synergism between the inorganic precursors and the organic matrix present in the biomineralization medium leads to materials with enhanced mechanical resistance and distinctive optical properties as compared to their synthetic counterparts.[2,3] This is greatly exemplified by bone, a biohybrid material recently described as a fractal-like organization.[4] At the mineralization front, bone mineral is deposited as nanometric crystals with a platelet morphology and their $c$ axis coaligned along the type I collagen fibrils.[5,6]

The preferred orientation of apatite crystals within the organic matrix and the development of pathological calcification driven by the deficiency in specific biomolecules strengthen their control over the nucleation and growth processes.[7,8] However, the exact role of organic molecules on bone mineralization is still under debate.

Type I collagen (30 wt.% of bone and 90 wt.% of the organic components in bone) is described to nucleate bioapatite by binding $Ca^{2+}$ on its charged amino acids residues.[9–11] Moreover, the assembly of collagen molecules into a dense and fibrillar matrix provides a confined environment *i.e.* inter- and intrafibrillar spaces, that also support the supersaturation of the ionic precursors of bone mineral.[12] Indeed, the structure, the size and the three-dimensional distribution of bioapatite at larger length scales are described to arise due to confinement effects.[12,13]

In addition to collagen, non-collagenous proteins (NCPs) and other type of organic species such as citrate are also reported to be involved in time and space in the mineralizing front of bone.[14–16] Among the NCPs, osteopontin, osteocalcin and osteonectin are proposed to control the

nucleation of amorphous calcium phosphate (ACP) and its further conversion into apatite.[17–19] A common characteristic of the selected NCPs is the presence of carboxylic acidic groups that create a high density of negatively charged domains with chemical affinity for $Ca^{2+}$ and apatite surface. In this sense, calcium-binding polymers have been extensively used to mimic NCPs, specially poly(aspartic acid) (pAsp), leading to the observation of a polymer induced liquid precursor (PILP).[20–22] *In vitro* studies have demonstrated that pAsp forms negatively charged ACP complexes that infiltrate the gap zones by interacting with positively charged domains in the collagen fibrils at the early stages of apatite mineralization.[11,23,24]

Citrate is an abundant component of the bone organic matrix (2 wt.% of bone or 5 wt.% of the organic components) that plays multiple roles on bioapatite mineralization.[25–27] Solid state nuclear magnetic resonance (ssNMR) studies evidenced citrate as an interfacial and strongly bounded molecule in bone.[28,29] It was proposed that citrate binds to the facets of apatite crystals preventing disordered growth thus controlling bone mineral in terms of size and morphology.[30–33] Apart from this, citrate foster the nucleation of ACP and its subsequent intrafibrillar mineralization by decreasing the interfacial energy between collagen and the mineral *in vitro*.[34]

Although the involvement of the collagen matrix, citrate and NCP appear clear, the way they act in space and time in bioapatite formation remains as a fundamental question. This may be partially explained by the fact that the use of high non-physiological concentrations of organic additives tends to stabilize kinetic CaP phases that are maybe not found in bone. Still, most studies on biomineralization rely on *ex situ* characterization of the products, which may lead to structural changes in the metastable phases due to dehydration during the isolation process and analysis. Thus, combining *in situ* to *ex situ* studies is of high interest to strengthen the conclusions.

Considering the challenges in probing the kinetic of the mineralization process, herein, *in situ* Raman and *ex situ* solid-state nuclear magnetic resonance (ssNMR) were used to depict the formation and structural evolution of biomimetic apatite in a bioinspired mineralization front containing collagen or the additives pAsp and citrate at varying concentrations. By doing so, it is possible to unveil the specific role of bone additives on the CaP precipitation (formation and stabilization). *In situ* Raman and *ex situ* ssNMR are non-invasive techniques allowing the study of CaP phases while preserving their hydration state and preventing from artifacts inherent of isolation processes. Strikingly, pAsp increases the lifetime of kinetic CaP intermediates while citrate at physiological concentrations stabilizes ACP. In contrast, collagen determines the structural properties of apatite regardless its concentration. Nevertheless, its role as organic scaffold in driving thermodynamically the apatite formation is only observed above the liquid-crystal threshold.

Unraveling the contribution of biomolecules during the pathway of mineral deposition and assembly in bone contributes significantly to the understanding of morphogenesis and further diseases caused by pathological mineralization; it also should be useful for the design of biomimetic materials with suitable properties.

## 2. EXPERIMENTAL

### 2.1 Formation of biomimetic apatite within a bioinspired mineralization front containing organic additives and collagen

#### 2.1.1 Precipitation in solution with citrate or pAsp

The organic additives pAsp or citrate were dissolved in acidic aqueous solution containing the ionic precursors of apatite $CaCl_2.2H_2O$ (110 mM, Sigma), $NaH_2PO_4$ (33 mM, Sigma), and $NaHCO_3$ (33 mM, Sigma). The Ca/(P + C) ratio was equal to 1.67 and the pH was adjusted to ~ 2.5 with hydrochloric acid 50 µg mL$^{-1}$ PolyAsp (L-aspartic acid sodium salt Bayer 1200 g mol$^{-1}$) was used according to the more common procedures found in the literature.[35] The content of citrate in bone is approximately 2% in mass.[25,27] Therefore, different concentrations of trisodium citrate (2.00, 0.25, 0.10 and 0.05 wt.% corresponding to 68.0, 8.3, 3.4 and 1.7 mM) were used in relation to the ionic precursors. As described previously, two flasks (35 mL, height = 50 mm) containing the mixtures (20 mL) and covered with perforated Parafilm were placed in a 1L beaker.[36] A third flask containing fresh aqueous ammonia solution (30 wt.%, 8 mL) was placed in the beaker that was sealed with Parafilm. $NH_3(g)$ diffusion into the flasks at ambient temperature slowly increases the pH of the solutions triggering the precipitation of calcium phosphate (CaP). After six days of reaction (pH~10-11), the solids were washed with distilled water then ethanol, to remove soluble salts and non-bonded molecules, centrifuged (6000 rpm, 10 min) and characterized. The CaP precipitation in the presence of organic additives was complementary monitored by *in situ* Raman and *ex situ* ssNMR. The control experiment, *i.e.* the precipitation of biomimetic apatite in the absence of additives in the same conditions, is described elsewhere.[37] ACP reference sample was prepared as described elsewhere.[38]

### 2.1.2 Precipitation in the presence of different concentrations of collagen

Different concentrations of collagen were used in the precipitation of apatite: a low one (2 mg mL$^{-1}$) according to the procedures commonly found in the literature and, higher concentrations to form organizations resembling those of the native (*i*) osteoid (40 mg mL$^{-1}$) and (*ii*) compact bone (250 mg mL$^{-1}$).[39] All the solutions were prepared in acetic acid (500 mM). Collagen was extracted from rat tail tendons following a classical procedure.[40] For the 2 mg mL$^{-1}$ system, the ionic precursors of apatite were dissolved in the collagen acidic solution (pH = 2.5). The 40 mg mL$^{-1}$ system was prepared by an evaporation procedure.[41] Accordingly, 100 mL of collagen acid solution (2 mg mL$^{-1}$) containing the ionic precursors of apatite was left open under a laminar flow hood for about 12 hours. This allows the evaporation of the acetic acid/water present in the solution leading to the desired concentration of collagen. 250 mg mL$^{-1}$ collagen matrices were formed using a procedure described elsewhere which combines injection and reverse dialysis.[12,42] Succinctly, an acidic collagen solution at low concentration (~2 mg mL$^{-1}$) is continuously injected in a disk-shaped dialysis chamber which is in contact with a polyethylene glycol solution (molecular weight cut off of 12-14 kDa). The polyethylene glycol solution is prepared by dissolving the polymer (PEG, 35 kDa, Fluka) in the acidic solution containing ionic precursors of apatite that was used for collagen. The concentration of the PEG solution controls the final concentration of collagen in the chamber. For all the samples, both fibrillogenesis of collagen and precipitation of mineral were trigged by the increase of pH to a range of 10 by $NH_3$ diffusion. The collagen concentration was determined by hydroxyproline titration.[43] The temporal evolution of mineral in the 250 mg mL$^{-1}$ system was investigated *ex situ* by ssNMR. To this end, the reaction was stopped at different intervals of time and the mineral characterized immediately

by $^{31}P$ ssNMR. The 2 mg mL$^{-1}$ and 40 mg mL$^{-1}$ systems were investigated *in situ* by Raman spectroscopy.

## 2.2 Fresh bone sample

Bone was extracted from the proximal part of the diaphysis and distal epiphysis of the humerus and femur from 2-year-old healthy French sheep. The study was reviewed and approved by the IMM Recherche's Institutional Animal Care and Use committee (IACUC) prior to starting. The animal research received an agreement (n°75-14-01) on September 08$^{th}$, 2013 for a period of 5 years by the "Sous-Direction de la protection Sanitaire" of the French Authorities.

## 2.3 Following the precipitation of biomimetic apatite *in situ* using micro-Raman spectroscopy

*In situ* Raman spectroscopy was used to monitor the evolution of CaP precipitation. The spectra were acquired with a KAISER Optical system equipped with a charge coupled detector (CCD) and a LASER with $\lambda = 785$ nm (P = 10-12 mW, resolution = 4 cm$^{-1}$ accumulation time = 150 seconds, 6 scans per spectrum, 1 spectrum every 16 minutes) using a fiber optic Raman probe equipped with a sapphire optical lens. The probe was immersed directly in the upper 2/3 of the ionic solution of one of the two flasks. $NH_3(g)$ was then introduced, and the chamber closed. The probe was maintained fixed during the precipitation to avoid artefacts. A homemade optical set up was used in the presence of collagen due to optical perturbations induced by the precipitation of fibrils. The set-up allows remote analysis from the optical head (MR-Probe-785) of the Raman spectrometer (Kaiser optical systems, Raman analyzer RXN1). The device is based on a principle similar to that of the immersion probe and involves a mounting that was screwed onto the optical head and consists of an aluminum tube with threaded ends carrying a 10x lens. The whole assembly

was wrapped with PTFE as illustrated in **Figure S1**. Spectral analysis and decompositions were performed using GRAM/AI software.

**2.4 *Ex situ* characterization**

The final products were isolated, washed with ultra-pure water and dried at 37°C, then characterized as follow.

*Ex situ micro-Raman*. After 6 days of reaction the final products were characterized *ex situ* by micro-Raman using a KAISER Optical system equipped with a charge coupled detector (CCD) and a LASER with $\lambda$ = 785 nm (P = 10-12 mW, resolution = 4 cm$^{-1}$ accumulation time = 20 s, 5 scans per spectrum) coupled with a microscope with a 50x lens.

*Transmission electron microscopy*. A transmission electron microscope (TEM JEOL 2011) operating at 200 keV was used to obtain the TEM images. To this end, the samples were dispersed in ethanol and some drops were deposited on a lacey carbon film on copper grid.

*Solid state NMR*. $^1$H and $^{31}$P ssNMR experiments were conducted on an Avance 500 Bruker spectrometer operating at $\nu$($^1$H) = 500.13 MHz, $\nu$($^{31}$P) = 202.40 MHz and $\nu$($^{13}$C) = 125.03 MHz. The t90°($^1$H), t90°($^{31}$P) and t90°($^{13}$C) were set to 4.5 $\mu$s , 5.5 and 5.5 $\mu$s, respectively. The powders were packed in 4 mm zirconia rotors and spun at 8-14 kHz. $^{31}$P direct acquisition spectra were recorded in quantitative conditions used a recycle delay (RD) of 200 s and a 30° pulse, the number of scans (NS) were set to 80. The 2D $^1$H-$^{31}$P HetCor spectra were recorded using the following parameters RD = 2 s; contact time $t_{CP}$ = 1 ms, NS = 32-80 for each 40-120 $t_1$ increments depending on the sample. The $^1$H-$^{13}$C CP MAS spectra were recorded using a contact time of 1 ms. The chemical shifts were referenced (0 ppm) to H$_3$PO$_4$ 85 wt.% for $^{31}$P and TMS for $^1$H and $^{13}$C.

# 3. RESULTS

## 3.1 Effect of pAsp on CaP precipitation

Precipitation and subsequent conversion of CaP phases over the mineralization process were tracked by following *in situ* the evolution of the $v_1PO_4$ band (symmetric stretch) in the Raman spectra (**Figure 1A**). Without any additives (referred as "control" experiment), the precipitation of biomimetic apatite occurs through the following sequence: amorphous calcium phosphate (ACP, 1.5h), octacalcium phosphate (OCP, 2.5h), CHA (> 10h).[37]

In the presence of pAsp, a weak and broad band at 951 cm$^{-1}$ ascribed to the $v_1PO_4$ typical of ACP is observed in the Raman spectrum after 11h. This higher induction time compared to that observed for the control experiment evidences the inhibitory effect of pAsp on the nucleation of CaP. After 19h, the arising of two shoulders at 953 and 962 cm$^{-1}$ shows the crystallization of ACP into OCP. The sharpening of the main band (FWHM = 17 *vs*. 14 cm$^{-1}$) occurring with time (18-22h) indicates that OCP becomes more crystalline upon maturation. Sequentially (from 25h), the OCP characteristic shoulder at 962 cm$^{-1}$ disappears indicating the transformation of OCP into a poorly crystalline apatite. As the mineralization proceeds (> 25h), the hydroxyapatite maturation is revealed by the sharpening of the $PO_4^{3-}$ band and the shift towards 958 cm$^{-1}$.

After 6 days of reaction, the product (CHA-pAsp) was isolated and characterized *ex situ* to investigate the effects of pAsp on the structure (**Figure 1B-C**) and morphology (**Figure 1D**) of apatite. Observations on TEM (Figure 1D) shows that CHA-pAsp is composed of aggregated platelets resembling to that found without additives (CHA) (**Figure S2A**). The *ex situ* micro-Raman spectra of CHA and CHA-pAsp are compared in Figure 1B. No significant differences (position, FWHM of $v_1PO_4$) were noted which suggests that pAsp did not impact on the structural features of biomimetic apatite. The direct $^{31}P$ MAS NMR spectrum for CHA-pAsp displays a main

signal at $\delta(^{31}P)$= 2.8 ppm typical of $PO_4^{3-}$ in apatitic environment (Figure 1C, red line). The $^{1}H\rightarrow^{31}P$ CP MAS spectra were also recorded for CHA-pAsp ($t_{cp}$ = 1 ms; Figure 1C, blue line). This experiment evidences protonated chemical environments around $^{31}P$ thanks to magnetization transfer from protons in spatial proximity. The $^{1}H$-$^{31}P$ CPMAS spectrum emphasizes two extra resonances ascribed to $HPO_4^-$ from OCP at $\delta(^{31}P)$ ~1.5 and ~ −0.3 ppm. According to previous investigations of reference samples[37], the proportion of OCP is estimated to 10%. The asymmetric resonance on the left side (red arrow) is evidenced using such short $t_{cp}$ and is related to the contribution of the amorphous layer of apatite and to a less extend to ortho-phosphate sites in OCP. Notably, OCP is not detected in the $^{31}P$ ssNMR spectra of the control emphasizing the ability of pAsp to stabilize this intermediate phase of CHA (**Figure S2B**).
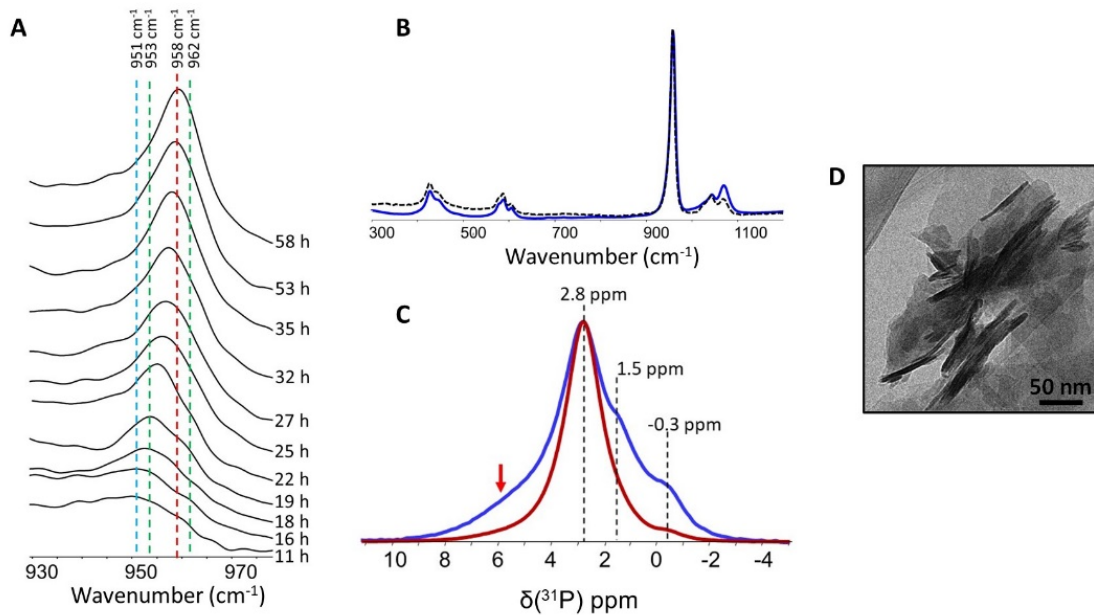
**Figure 1.** Formation of apatite in the presence of 50 µg mL$^{-1}$ pAsp. (A) *In situ* monitoring of mineralization by Raman spectroscopy. The blue line (951 cm$^{-1}$), green lines (953 and 962 cm$^{-1}$) and red line (958 cm$^{-1}$) represent the ACP, OCP and the apatite contributions, respectively. (B) Comparison between *ex situ* micro-Raman spectra of CHA-pAsp (blue line) and CHA (dashed black line). (C) Quantitative $^{31}$P MAS NMR (red line) and $^{1}$H→$^{31}$P CP MAS (t$_{cp}$= 1 ms; blue line) spectra of CHA-pAsp. The asymmetric resonances on the right correspond to HPO$_4^{2-}$ from OCP and on the left side (red arrow) is related to the contribution of the amorphous layer of apatite and to a less extend to ortho-phosphate sites in OCP. (D) TEM images of CHA-pAsp.

12

## 3.2 Effect of citrate on CaP precipitation

We first investigated the precipitation of biomimetic apatite in the presence of 2 wt.% citrate, which is the concentration described in bone (**Figure 2A**).[25,27] At t=0, the *in situ* Raman spectrum displays a large band in the region of 900-940 cm$^{-1}$ assigned to the carbon—carbon stretching modes $v$(C—COO) from citrate chain.[44] After 3h, a shoulder at 951 cm$^{-1}$ is observed indicating the formation of ACP. The longer induction time in comparison with the control (1.5h) shows that citrate delays the nucleation of CaP. This band intensifies as the reaction proceeds (at least for 27h) indicating the stabilization of ACP. The same precipitation pathway is found when the concentration of citrate is about 10 times lower than that found *in vivo* (0.25 wt.%) and ACP is not converted into apatite at least during the *in situ* Raman monitoring (**Figure 2B**). Then, the reaction was performed for 6 days and the products were isolated and characterized by *ex situ* TEM, ssNMR and micro-Raman spectroscopy. The Raman spectra of a pure ACP sample and the isolated products precipitated in the presence of 2 wt.% citrate (ACP-cit2%) and 0.25 wt.% citrate (ACP-cit0.25%) are compared in **Figure 2C**. The similarities between the spectra of ACP-citrate and pure synthetic ACP samples confirm the stabilization of amorphous precursor even after 6 days of reaction. Notably, ACP-cit2% displays larger Raman band as compared to ACP-cit0.25% indicating a higher degree of disorder. The $^{31}$P MAS NMR spectrum of ACP-cit0.25% (red line) shows a resonance peak centered at δ ($^{31}$P) = 3.2 ppm typical of ACP (**Figure 2D**). In addition, the broadening of the $^{31}$P resonance seen on the $^{1}$H-$^{31}$P CP MAS NMR spectrum (t$_{cp}$= 1 ms; blue line) evidences the contribution of protonated phosphates and/or water molecules. Interestingly, ACP-cit0.25% seems more structured than pure synthetic ACP because of its smaller line width (FWHM = 4.75 *vs* 5.80 ppm).

TEM images reveal that ACP-cit0.25 displays particles with irregular morphology typical of ACP (**Figure 2E, E'**). The presence of citrate in ACP-cit2% was investigated by $^{13}$C ssNMR. **Figure S3** compares the H-$^{13}$C CP MAS NMR spectra of crystallized citrate used as reference (red line) and ACP-cit2% (green line). Resonances peaks typical of citrate are observed in ACP-cit2%: the signals at $\delta$ ($^{13}$C) = 180.4, 76.5 and 47.6 ppm are assigned to carboxylic group, quaternary carbon and CH$_2$ groups, respectively.[29] The resonance at $\delta$ ($^{13}$C) = 168.5 ppm ascribed to inorganic carbonate is also observed. This result indicates the presence of citrate on the surface and/or inside the core of the mineral in ACP-2%cit.
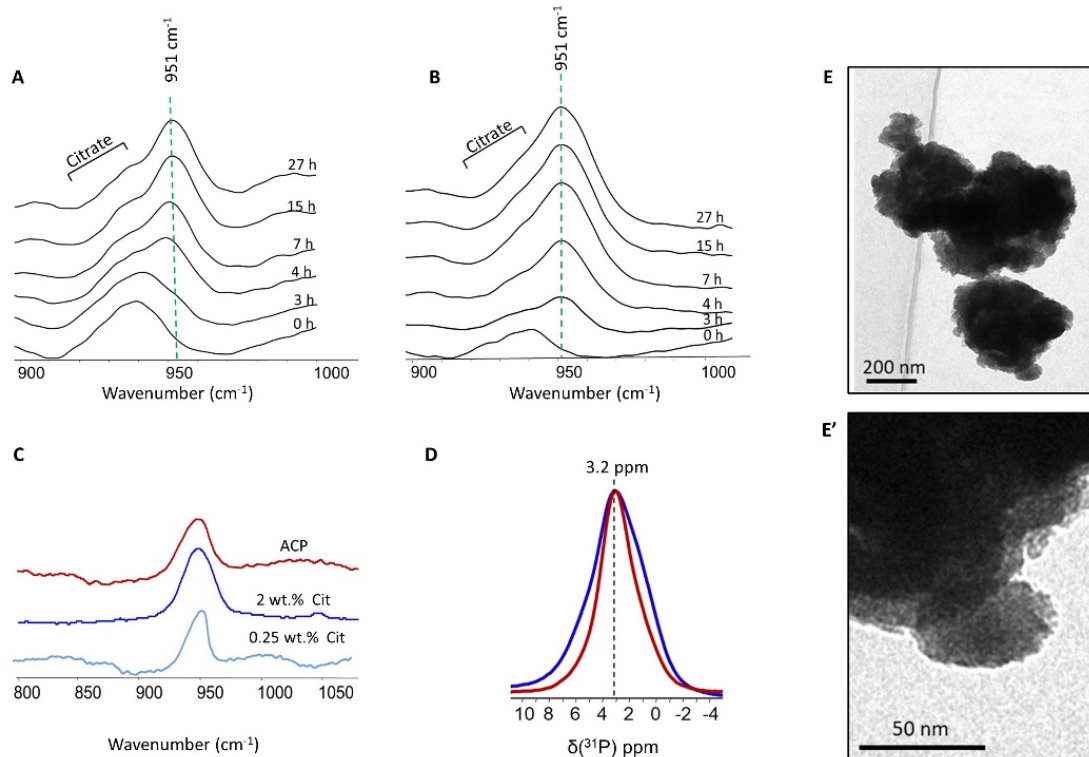
**Figure 2.** Formation of apatite in the presence of 2wt.% and 0.25 wt.% citrate. (A) and (B) *In situ* monitoring of mineralization by Raman spectroscopy of the systems containing 2wt.% and 0.25 wt.% citrate, respectively. The blue line at 951 cm$^{-1}$ and the band at 940 cm$^{-1}$ represent the ACP and citrate contributions, respectively (C) Comparison of the *ex situ* micro-Raman spectra of ACP-Cit0.25% (light blue line) with ACP-Cit2% (blue line) and ACP (red line). (D) $^{31}$P ssNMR spectra of ACP-cit0.25%. Quantitative $^{31}$P MAS (red line) and $^{1}$H$\rightarrow^{31}$P CP MAS ($t_{cp}$= 1 ms , blue line) spectra of ACP-cit0.25%. (E and E') TEM images of ACP-cit0.25%.

Experiments at lower concentrations of citrate (about 20 and 40 times lower than that found *in vivo*) were then conducted to evaluate the ability of this additive to stabilize ACP. At 0.1 and 0.05 wt.% citrate, the bands around 940 cm$^{-1}$ assigned to carbon-carbon stretching bands are not detected in the Raman spectra due to low citrate concentration (**Figure 3A-B**). The broad $v_1PO_4^{3-}$ band at 951 cm$^{-1}$ typical of ACP is observed after ~5h of reaction for both samples. This induction time is comparable with the 2 and 0.25 wt.% systems (~3h, Figure 2A-B) indicating that citrate concentration (in the 0.05-2 wt.% range) does not play a significant role in the kinetic of ACP nucleation. Then, ACP transforms into apatite with time ($v_1PO_4$ band shift to 957 cm$^{-1}$). However, this conversion is faster for 0.05 wt.% citrate: the full conversion is reached after 95 and 24h for 0.1 and 0.05 wt.% citrate, respectively. Finally, OCP bands are not observed indicating that OCP did not precipitate or its concentration is lower than 10 w%.[37]

After 6 days of reaction, the apatite formed in the presence of 0.05 wt.% citrate (CHA-cit0.05%) was isolated and characterized by *ex situ* micro-Raman, ssNMR and TEM (**Figure 3C-E**). Large aggregates of platelets are observed by TEM (Figure 3C). Observations at higher magnification show that the platelets are similar to CHA in terms of size and morphology (Figure 3C').[36] The way they organize is in agreement with previous observations showing that citrate may favor oriented attachment of apatite crystals.[45] However, the fact that (*i*) TEM observations were performed under vacuum and (*ii*) such alignment is observed for CHA without any additives[46] precludes conclusions on the role played by citrate on the particles' aggregation. The *ex situ* micro-Raman spectra of CHA and CHA-cit0.05% are similar in terms of $PO_4$ bands position and linewidth except for the band at 1070 cm$^{-1}$ which is more intense and consistent with the presence of citrate (**Figure 3D**). This indicates that this additive does not induce major structural changes in apatite as confirmed by the $^{31}P$ MAS NMR spectrum where $PO_4^{3-}$ is in a similar chemical

environment in both samples (Figure 3E red line *vs*. **Figure S2**). Additionally, no contribution related to OCP was detected in the $^1$H-$^{31}$P CP NMR spectrum, which is consistent with the Raman results. This indicates that citrate allows the direct conversion of ACP into hydroxyapatite. Spectra recorded using short contact times evidence the contribution of $HPO_4^{2-}$ from the amorphous layer in the mineral (red arrow), also reported for biomimetic and bone apatite.[46]
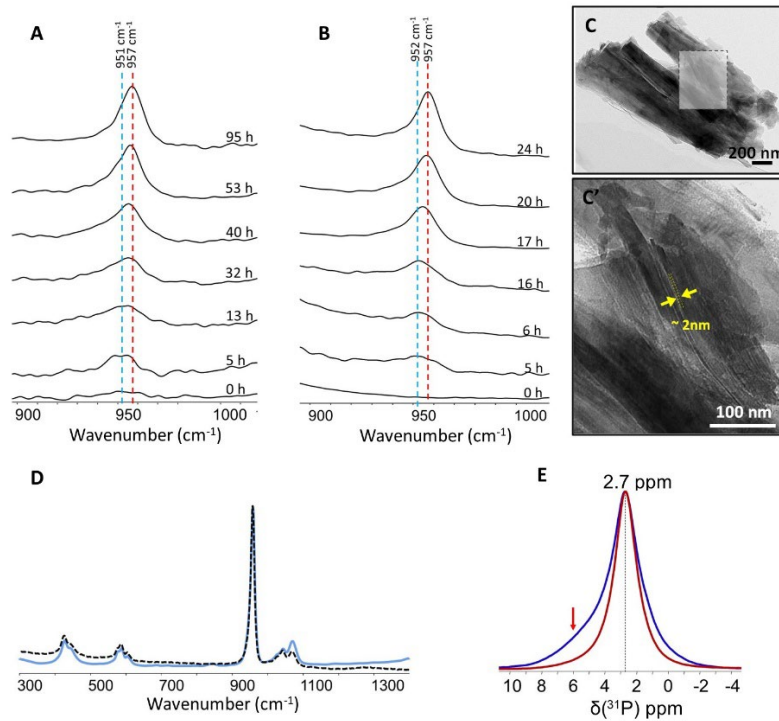
**Figure 3.** Formation of apatite in the presence of 0.1 wt.%. and 0.05 wt.%. citrate. (A) and (B) *in situ* monitoring by Raman spectroscopy of mineralizing systems containing 0.1wt.% and 0.05 wt.% citrate, respectively. The blue line at ~951 cm$^{-1}$ and the red band at ~957 cm$^{-1}$ represent the ACP and apatite citrate contributions, respectively. (C, C') TEM images of CHA-cit0.05%. (D) Comparison between Raman spectra of CHA-cit0.05% (blue line) and CHA (black dashed line). (E) ^{31}P ssNMR spectra of CHA-cit0.05%. Quantitative ^{31}P MAS (red line) and [1]H-^{31}P CP MAS (t$_{cp}$= 1 ms; blue line) spectra.

### 3.3 Effect of collagen on CaP precipitation

Two concentrations were first used for collagen, a low (2 mg mL$^{-1}$) and a high (40 mg mL$^{-1}$). The higher one tends to mimic the environment in the biological osteoid tissue in terms of collagen concentration.[47] In both cases, a band at 888 cm$^{-1}$ ascribed to the stretching vibration mode of the carbonic chain from acetic acid is observed in the Raman spectra (**Figure 4A-B**). As the reaction evolves through the increase of pH, this band vanishes while a new arising band ascribed to acetate ion is detected at 927 cm$^{-1}$. Importantly, there is no collagen bands observed in the PO$_4$ region.

The 2 mg mL$^{-1}$ system was first investigated (Figure 4A). A typical band of ACP at 950 cm$^{-1}$ is observed after 2h. The displacement of the band towards 958 cm$^1$ (between 10h and 172h) is ascribed to the progressive transformation of ACP into apatite. The sequentially band sharpening indicates that apatite undergoes maturation.

No major changes in the pathway of apatite formation are detected for the 40 mg mL$^{-1}$ system (Figure 4B) compared to the 2 mg mL$^{-1}$. This is in agreement with the precipitation of spherulitic crystals in both systems (**Figure 4C-D**).[48]

After 6 days of reaction, the products were isolated and characterized. The *ex situ* micro-Raman spectra of CHA-col/2mg mL$^{-1}$ and CHA-col/40mg mL$^{-1}$ (blue in **Figure 4E** and **4F**, respectively) are compared to CHA and fresh bone. Typical bands of apatite are observed in the range of 400-1100 cm$^{-1}$ namely $v_1PO_4$ = 950 cm$^{-1}$ and $v_2PO_4$ = 410 cm$^{-1}$, $v_3PO_4$ = 1010 cm$^{-1}$ and $v_4PO_4$ = 550 cm$^{-1}$. Collagen bands are observed around 1200 cm$^{-1}$. Apatite in the samples containing collagen and fresh bone sample display similar spectral signature in terms of position and linewidth of the $v_1PO_4$band, regardless the concentration of collagen (FWHM bone = 18 cm$^{-1}$, FWHM CHA-col/2mg mL$^{-1}$, = 17 cm$^{-1}$, FWHM CHA-col/40mg mL$^{-1}$ = 17 cm$^{-1}$). Conversely,

pure CHA is characterized by sharper phosphate bands indicating a higher crystallinity (FWHM = 12 cm$^{-1}$). The *ex situ* $^{31}$P CP MAS ssNMR spectra of CHA-col 40mg mL$^{-1}$ (blue line) and pure CHA (red line) are compared in **Figure 4G**. CHA-col 40mg mL$^{-1}$ displays a resonance peak at $\delta(^{31}P) = 3.0$ ppm characteristic of biological apatite together with a shoulder on the left indicative of amorphous layer and/or remaining ACP phase.
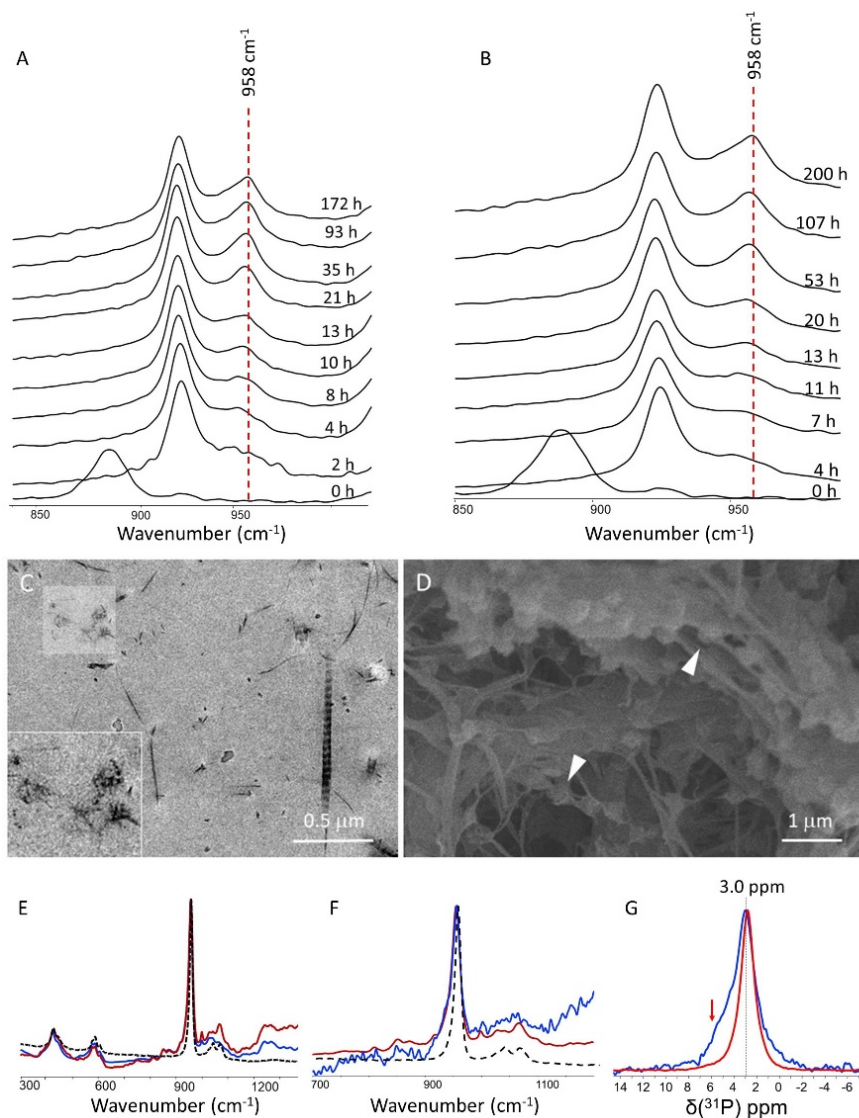
**Figure 4.** Formation of apatite in the presence of collagen 2 mg mL$^{1-}$ and 40 mg mL$^{-1}$. (A) and (B) *In situ* monitoring of mineralization by Raman spectroscopy of the systems containing 2 mg mL$^{1-}$ and 40 mg mL$^{-1}$ collagen, respectively. The red band at ~958 cm$^{-1}$ corresponds to the apatite contributions. (C) TEM of ultrathin section of CHA-col/2mg mL$^{-1}$ and (D) SEM micrographs of CHA-col/40mg mL$^{-1}$; for both, apatite crystals aggregate into spherulites (white arrows). The light square in C indicates the enlarged section that is shown in the inset. (E) Comparison of the Raman spectra of CHA-col/2mg mL$^{-1}$ (blue line) with CHA (black dashed line) and fresh bone (red line). (F) Comparison between the Raman spectra of CHA-col/40mg mL$^{-1}$ (blue line), CHA (black dashed line) and fresh bone (red line). (G) $^{31}$P CP MAS NMR spectrum (t$_{CP}$ = 1 ms) of CHA-Col/40mg mL$^{-1}$ (blue line) and CHA (red line).

Because osteoid tissue is not mineralized, further investigations were performed with a collagen concentration that mimics the suprafibrillar arrangement of mature bone (250 mg mL$^{-1}$, **Figure 5**).[12] *In situ* Raman investigations were performed in the presence of apatite ion precursors but the high collagen concentration did not allow the observation of phosphate bands in the 940-990 cm$^{-1}$ region (**Figure S4**). Therefore, the time evolution of minerals within the 250 mg mL$^{-1}$collagen matrix was only investigated by *ex situ* $^{31}$P ssNMR (**Figure 5A**).

At t=0, a single narrow signal ascribed to free phosphate species in solution is observed at $\delta(^{31}P)$ = 0.03 ppm (mainly $H_3PO_4/H_2PO_4^-$ at pH ~2) with a line width of FWHM = 45 Hz. After 0.5h, the pH increases through $NH_3$ diffusion and the resonance peak shifts to 2.7 ppm, although the linewidth remains unchanged. This is ascribed to the formation of hydrogenophosphate species (HP) related to the loss of protons in the solution. Surprisingly, this ionic species did not precipitate remaining stable in the alkaline environment until 48h, which contrasts with the previous systems. Indeed, ACP forms after 72h as observed by the position $\delta(^{31}P)$ = 3.0 and the typical broad gaussian line shape (FWHM = 4.2 ppm). This induction time is much longer than that found in the control (1.5h), pAsp (11h), citrate 2.0 wt.% (3h) and citrate 0.0.5 wt.% (5h). Finally, the signal-narrowing is observed after 100 h resulting in a resonance peak at $\delta(^{31}P)$ = 2.9 with FWHM = 1.85 ppm that reflects the crystallization of ACP into apatite. Although the linewidth is smaller to that found for bone mineral (2.95 ppm), it is higher than that found for CHA-col 40 mg mL$^{-1}$ (1.5 ppm) and for pure CHA (1.65 ppm). These results reflect the effect of collagen confinement (*i.e.* high fibrils density, **Figure 5B**) on both apatite structure and dispersion in CHA-Coll 250 mg mL$^{-1}$ as previously shown in the literature.[11,49] As seen in Figure 4D, spherulites are observed in low concentrated matrix while single particles co-align with collagen (white arrows) at bone-like concentration as observed by TEM (**Figure 5C**). Note that the ultrathin section is not stained to

avoid any misleading of interpretation between heavy metals and apatite particles as previously shown.[12]

2D $\{^1H\}^{31}P$ HetCor NMR experiments were performed to characterize the mineral formed after 72h (**Figure 5D**). Noticeably, the $^{31}P$ projections reveal the presence small amount of hydroxyapatite. Indeed, two distinct signals with similar chemical shifts $\delta(^{31}P) = 3.2$ ppm are observed with different linewidths: one sharp (2.9 ppm) that correlates with hydroxyl anions at $\delta(^1H) = 0$ ppm and one broad and more intense (3.0 ppm) that correlates with water molecules at $\delta(^1H) = 4.85$ ppm. Interestingly, although this suggests the coexistence of ACP and apatite in the sample formed after 72h one cannot exclude the formation of apatite crystals with a high amorphous layer/crystalline core ratio. Indeed, first, the collagen/ACP signature is thinner than that of pure ACP particles in terms of linewidth (FWHM = 4.2 ppm *versus* 5.8 ppm, respectively) and second, ACP resembles the amorphous layer found in bone mineral and biomimetic apatite in terms of chemical shift $\delta(^{31}P)$ ACP/Col= 3.1 ppm, $\delta(^{31}P)$ ACP/bone (3.2 ppm) and $\delta(^{31}P)$ pure ACP = 3.4 ppm.
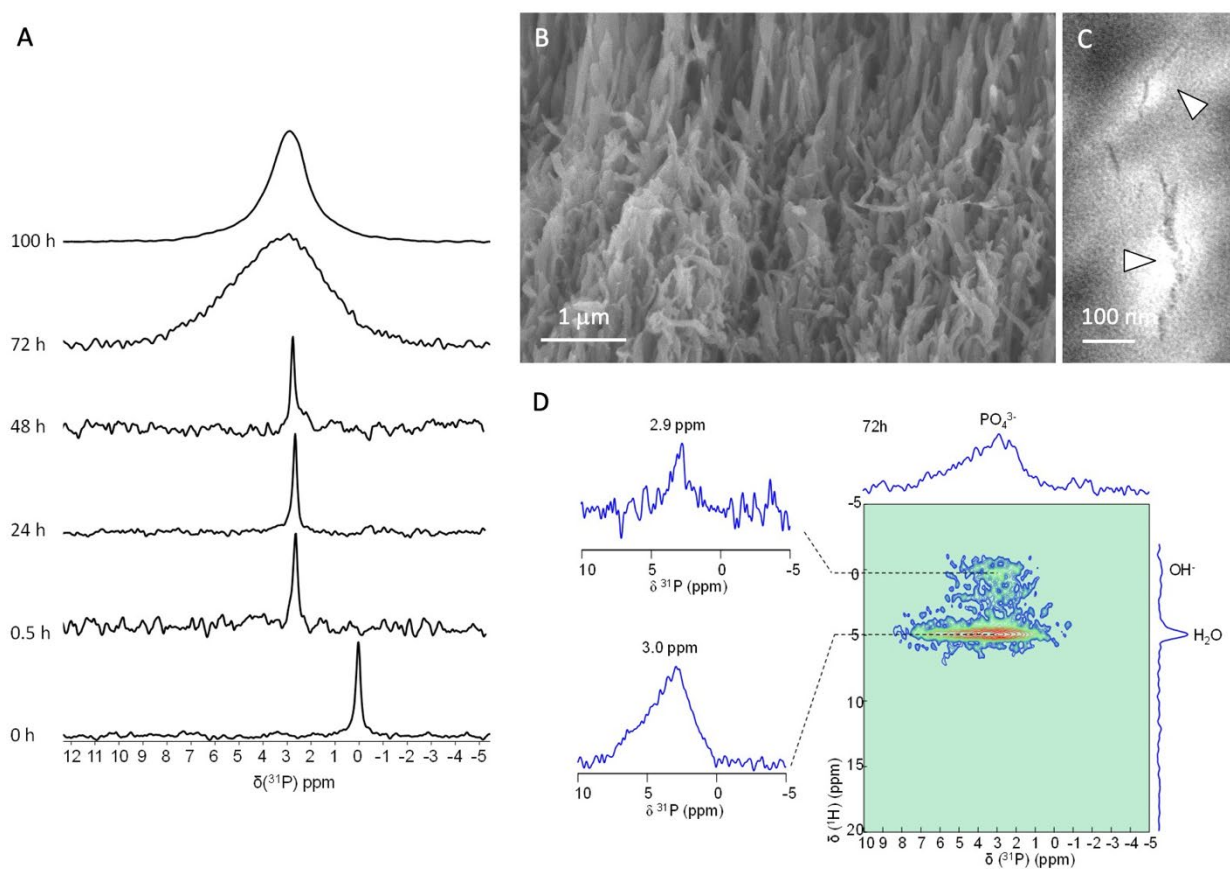
**Figure 5.** Formation of apatite in dense collagen matrix (250 mg mL$^{-1}$). (A) *Ex situ* monitoring of mineralization by $^{31}$P ssNMR. (B) SEM and (C) TEM images of unstained CHA-Col/250 mg mL$^{-1}$ section showing the high density of collagen fibrils forming a confined environment where CHA crystals co-aligned with collagen (white arrows) as described in bone. (D) 2D $^{1}$H–$^{31}$P HetCor experiment (1 ms contact time) recorded after 480 min together with $^{31}$P 1D spectra extracted at $\delta(^{1}$H) = 0 ppm (hydroxyl from CHA) and $\delta(^{1}$H) = 5 ppm (water molecules from ACP).

## 4. DISCUSSION

The kinetics of CaP precipitation described above for pAsp, citrate and collagen are schematically summed-up in **Figure 6**. ACP is the first phase to form in the presence of citrate, pAsp and collagen regardless their concentrations as predicted by the Ostwald's step rule.[50,51] Compared to the control, the kinetic of ACP formation is slowdown in presence of all additives probably due to the binding of $Ca^{2+}$ to the negatively charged moieties.[52,53] However, we need to emphasize that aside $Ca^{2+}$, the role of phosphate is so far neglected as discussed earlier.[75] The formation of ACP at the early stages of bone mineralization proposed by Termine and Posner is commonly accepted.[54] However, amorphous precursors remain debated in biomineralization and the nature of the first mineral phases deposited during bone formation remains as an unanswered question.[55–59]

The nature and lifetime of the CaP intermediates *in vitro* is controlled by the nature and concentration of the additives, *e.g.* brushite is not detected and OCP is rarely found in the present work. pAsp is shown to enhance the stability of ACP with respect to OCP in the control experiment, as evidenced by both *in situ* Raman and $^{31}P$ ssNMR. Conversely, in the presence of citrate (0.05 wt.%) and collagen, ACP crystallizes directly into apatite without forming OCP. These results suggest that the additives modify kinetic and mechanism by which apatite forms. Indeed, citrate has been shown to stabilize apatite over other CaP phases *i.e.* OCP and brushite, possibly by different mechanisms including a decrease in the surface energy barrier[28], a spatial citrate/apatite crystallographic match[29], and a selective binding between $Ca^{2+}$ and carboxyl group of citrate.[60] Here, the noticeable difference between collagen and citrate is the lifetime of ACP. Indeed, collagen leads to the formation of a transient ACP while citrate prevents ACP from crystallization at physiological concentration (for t<6 days). $^{31}P$ and $^{13}C$ ssNMR confirms the

binding of citrate ions onto the surface of ACP which is reported to decrease the exposition of the mineral to the solution[44] and to stabilize it in solution thanks to electrostatic repulsion.[61]

Strikingly, precipitations in the presence of different concentrations of collagen revealed that highly concentrated matrices with a cholesteric geometry typical of compact bone stabilizes an ionic species prior to the nucleation of ACP-apatite. This suggests that collagen acts either as additives or as organic scaffold below and above the liquid-crystal threshold, respectively. The observation of such long-term stabilized ionic species suggests a steady-state local phosphate supersaturation induced by collagen suprafibrillar organization raising interesting questions regarding the role of collagen concentration on bone mineralization. It is not possible to distinguish whether ACP is found as transient apatite precursor phase or as a surface layer of apatite[43] by the $^1H$-$^{31}P$ HETCOR spectra but it is worth mentioning that a high amorphous layer/crystalline core ratio decreases upon apatite maturation *in vitro*[62] and in biological system (bone and enamel).[63] Several studies have shown that NCPs and charged polymers can inhibit the nucleation and growth of apatite and promote the ACP formation.[14,64] Herein, in addition to the *in situ* investigation of the mechanisms by which biological molecules alter the pathway of apatite mineralization, we also evaluated its impact on the structure of apatite. A fresh bone sample was used to strengthen the results.

The apatite platelets form in the presence of citrate exhibit a lateral alignment as observed by TEM (Figure 3C-C') in agreement with previous observations showing that it favors the oriented attachment of mineral crystals in bone.[29,31,45] This also emphasizes that this molecule strongly interacts with the surface of minerals as showed by the ssNMR results.[65,66] Besides the coordination between the negatively charged carboxylate groups and the $Ca^{2+}$ ions, citrate binding on the mineral surface can also take place *via* H-bonding with structural water and OH groups

forming the mineral.[67–69] Although Raman shows no differences between synthetic apatite (CHA) and CHA-cit, ^{31}P ssNMR reveals that the spectroscopic signature of amorphous layer in apatite tends to be closer to bone mineral in the presence of citrate (Figure 2 and 3).

It is worth mentioning that apatite mineral obtained in the presence of collagen is indistinguishable from fresh bone regardless its concentration strengthening that collagen itself directs the formation of bone apatite defining its structural properties. [9,10,12,70–72] This is ascribed to the combination of stereochemistry, charge and the 3D arrangement of collagen, that provide a structural template to the oriented nucleation and growth of apatite.

Therefore, one can hypothesize that inhibitors are needed to avoid pathological mineralization *in vivo*. Indeed, although the body fluid is supersaturated with respect to apatite, the deposition of mineral only takes place at specific tissues thanks to the combined action of initiators and inhibitors of mineralization. Biological molecules such as citrate and NCPs, paradoxically favor physiological mineralization by selectively preventing apatite growth in solution outside the collagen scaffold.[34,73,74] This is exemplified by the development of pathological calcification and the diversity of CaP phases found in stone diseases due to the deficiency of citrate (*i.e* hypocitraturia) and NCPs in the plasma and urine.[75–77] Additionally, these organic components are important for the transport of ionic precursors to the mineralization sites.[77,78] The carboxyl groups from the molecules chelate $Ca^{2+}$ forming negatively charged complexes which are attracted to the positively charged amino acids in collagen.[11] Hence, even though decreasing the concentration of free ions in solution, these complexes accumulate ionic precursors in the calcified organic matrix.[79,14]

All these results suggest that citrate and acidic calcium-binding NCPs are involved in the earliest stages of mineralization acting mainly in (*i*) the prevention of pathological mineralization and (*ii*)

the delivery of $Ca^{2+}$ rich complexes in the gap zones of collagen triggering locally the supersaturation towards apatite but are not crucial for the oriented growth of apatite. Complementary, current hypotheses consider a similar role for matrix vesicles which may transport and accumulate calcium and phosphate ions outside the cells, that further associate with the extracellular collagenous-based matrix.[80,81] Conversely, tissue-like concentration of collagen allows the formation of a biomimetic confinement that stabilizes transient ionic species even at alkaline pH. This possibly favors supersaturation of apatite ion precursors in specific sites leading to the collagen/apatite co-alignment as reported earlier.[12] Overall, these results show that collagen acts either as additives or as organic scaffold below and above the liquid-crystal threshold, respectively. This particularly meaningful since fibrils density increases from the non-mineralized osteoid to the highly mineralized mature bone tissues.[82]

It is important to note that the mineralization in biological systems is much more complex than *in vitro* models and that all these molecules should be present together with cells and a multitude of specialized molecules at different concentrations. In addition, other inorganic ions are found in bioapatite such as $Sr^{2+}$,[83] $Mg^{2+}$[84] or $F^-$[85] and may influence the precipitation pathway *in vivo*. In this respect, further investigations are needed to understand the interplay between such organic components.[86,87]
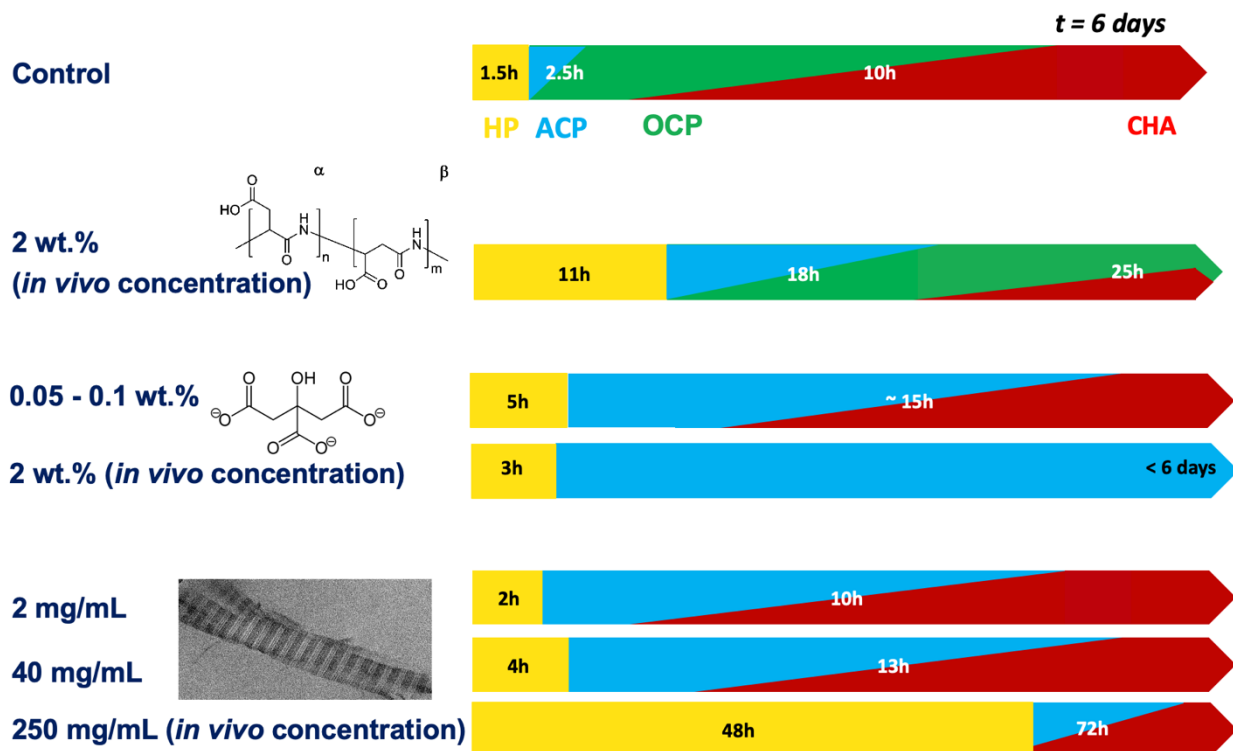
**Figure 6** Schematic representation of the time scales for CaP precipitation without additive (control), in the presence of pAsp, citrate and collagen (HP: hydrogenphosphate ions) during 6 days. Colours and the corresponding lifetime of CaP precursors are indicated in arrows: HP (yellow), ACP (blue), OCP (green) and CHA (red) during the CaP precipitation pathway.

# 5. CONCLUSIONS

By preserving the hydration state of both mineral and organic additives, we show here how concentration of biological components in models for bone mineralization can modulate the commonly accepted pathway of CaP precipitation, that is ACP, OCP and HAP. The synthetic pAsp stabilizes OCP while it is inhibited by citrate. At physiological-like concentration, citrate appears to preclude HAP precipitation which only forms at very low concentration. Collagen determines the structural properties of HAP regardless of its concentration. With biomimetic high collagen concentration, ionic species are stabilized prior to the nucleation of the mineral phase. Our work highlights that confinement drives thermodynamically HAP formation by slowing down the kinetic formation of CaP precursors and agrees with *in vivo* observations showing that « […] mineralization process of bone […] occurs very rapidly after the self-assembly of the collagen molecules to collagen fibrils […][88]

# 6. ACKNOWLEDGEMENTS

## 7. ASSOCIATED CONTENT

Additional schematic representation of the *in situ* Raman set up, TEM images, solid state NMR and Raman spectra.

## 8. REFERENCES

(1)     Lowenstam, H. A.; Weiner, S. *On Biomineralization.*; Oxford University Press on Demand, 1989.

(2)     Aizenberg, J.; Tkachenko, A.; Weiner, S.; Addadi, L.; Hendler, G. Calcitic Microlenses as Part of the Photoreceptor System in Brittlestars. *Nature* **2001**, *412* (6849), 819–822.

(3)     Marcus, M. A.; Amini, S.; Stifler, C. A.; Sun, C.-Y.; Tamura, N.; Bechtel, H. A.; Parkinson, D. Y.; Barnard, H. S.; Zhang, X. X. X.; Chua, J. Q. I.; et al. Parrotfish Teeth: Stiff Biominerals Whose Microstructure Makes Them Tough and Abrasion-Resistant To Bite Stony Corals. *ACS Nano* **2017**, *11* (12), 11856–11865.

(4)     Reznikov, N.; Bilton, M.; Lari, L.; Stevens, M. M.; Kröger, R. Fractal-like Hierarchical Organization of Bone Begins at the Nanoscale. *Science* **2018**, *360* (6388).

(5)     Weiner, S.; Wagner, H. D. The Material Bone: Structure-Mechanical Function Relations. *Annu. Rev. Mater. Sci.* **1998**, *28* (1), 271–298.

(6)     Blair, H.; Teitelbaum, S.; Ghiselli, R.; Gluck, S. Osteoclastic Bone Resorption by a Polarized Vacuolar Proton Pump. *Science* **1989**, *245* (4920), 855–857.

(7)     Ascenzi, A.; Bonucci, E.; Generali, P.; Ripamonti, A.; Roveri, N. Orientation of Apatite in Single Osteon Samples as Studied by Pole Figures. *Calcif. Tissue Int.* **1979**, *29* (1), 101–

105.

(8)     Quelch, K. J.; Cole, W. G.; Melick, R. A. Noncollagenous Proteins in Normal and Pathological Human Bone. *Calcif. Tissue Int.* **1984**, *36* (1), 545–549.

(9)     Landis, W. J.; Silver, F. H. Mineral Deposition in the Extracellular Matrices of Vertebrate Tissues: Identification of Possible Apatite Nucleation Sites on Type I Collagen. *Cells Tissues Organs* **2008**, *189* (1–4), 20–24.

(10)    Silver, F. H.; Landis, W. J. Deposition of Apatite in Mineralizing Vertebrate Extracellular Matrices: A Model of Possible Nucleation Sites on Type I Collagen. *Connect. Tissue Res.* **2011**, *52* (3), 242–254.

(11)    Nudelman, F.; Pieterse, K.; George, A.; Bomans, P. H. H.; Friedrich, H.; Brylka, L. J.; Hilbers, P. A. J.; De With, G.; Sommerdijk, N. A. J. M. The Role of Collagen in Bone Apatite Formation in the Presence of Hydroxyapatite Nucleation Inhibitors. *Nat. Mater.* **2010**, *9* (12), 1004–1009.

(12)    Wang, Y.; Azaïs, T.; Robin, M.; Vallée, A.; Catania, C.; Legriel, P.; Pehau-Arnaudet, G.; Babonneau, F.; Giraud-Guille, M. M.; Nassif, N. The Predominant Role of Collagen in the Nucleation, Growth, Structure and Orientation of Bone Apatite. *Nat. Mater.* **2012**, *11* (8), 724–733.

(13)    Xu, Y. F.; Nudelman, F.; Eren, E. D.; Wirix, M. J. M.; Cantaert, B.; Nijhuis, W. H.; Hermida-Merino, D.; Portale, G.; Bomans, P. H. H.; Ottmann, C.; Friedrich, H.; Bras, W.; Akiva, A.; Orgel, J. P. R. O.; Meldrum, F. C.; Sommerdijk, N. Intermolecular Channels Direct Crystal Orientation in Mineralized Collagen. *Nat. Commun.* **2020**, *11* (1), 1–12.

(14)    George, A.; Veis, A. Phosphorylated Proteins and Control over Apatite Nucleation, Crystal Growth, and Inhibition. *Chem. Rev.* **2008**, *108* (11), 4670–4693.

(15)    Deshpande, A. S.; Beniash, E. Bioinspired Synthesis of Mineralized Collagen Fibrils. *Cryst. Growth Des.* **2008**, *8* (8), 3084–3090.

(16)    Beniash, E.; Traub, W.; Veis, A.; Weiner, S. A Transmission Electron Microscope Study Using Vitrified Ice Sections of Predentin: Structural Changes in the Dentin Collagenous Matrix Prior to Mineralization. *J. Struct. Biol.* **2000**, *132* (3), 212–225.

(17)    Ibsen, C. J. S.; Gebauer, D.; Birkedal, H. Osteopontin Stabilizes Metastable States Prior to Nucleation during Apatite Formation. *Chem. Mater.* **2016**, *28* (23), 8550–8555.

(18)    Zhao, W.; Wang, Z.; Xu, Z.; Sahai, N. Osteocalcin Facilitates Calcium Phosphate Ion Complex Growth as Revealed by Free Energy Calculation. *Phys. Chem. Chem. Phys.* **2018**, *20* (18), 13047–13056.

(19)    Hoac, B.; Nelea, V.; Jiang, W.; Kaartinen, M. T.; McKee, M. D. Mineralization-Inhibiting Effects of Transglutaminase-Crosslinked Polymeric Osteopontin. *Bone* **2017**, *101*, 37–48.

(20)    Olszta, M. J.; Odom, D. J.; Douglas, E. P.; Gower, L. B. A New Paradigm for Biomineral Formation: Mineralization via an Amorphous Liquid-Phase Precursor. *Connect. Tissue Res.* **2003**, *44* (1), 326–334.

(21)    Thula, T. T.; Svedlund, F.; Rodriguez, D. E.; Podschun, J.; Pendi, L.; Gower, L. B. Mimicking the Nanostructure of Bone: Comparison of Polymeric Process-Directing Agents. *Polymers.* **2010**, *3* (1), 10–35.

(22)   Olszta, M. J.; Douglas, E. P.; Gower, L. B. Scanning Electron Microscopic Analysis of the Mineralization of Type I Collagen via a Polymer-Induced Liquid-Precursor (PILP) Process. *Calcif. Tissue Int.* **2003**, *72* (5), 583–591.

(23)   Jiao, K.; Niu, L. N.; Ma, C. F.; Huang, X. Q.; Pei, D. D.; Luo, T.; Huang, Q.; Chen, J. H.; Tay, F. R. Complementarity and Uncertainty in Intrafibrillar Mineralization of Collagen. *Adv. Funct. Mater.* **2016**, *26* (38), 6858–6875.

(24)    Zhou, Z.; Zhang, L.; Li, J.; Shi, Y.; Wu, Z.; Zheng, H.; Wang, Z.; Zhao, W.; Pan, H.; Wang, Q.; et al. Polyelectrolyte–Calcium Complexes as a Pre-Precursor Induce Biomimetic Mineralization of Collagen. *Nanoscale* **2021**, *13* (2), 953–967.

(25)   Dickens, F. The Citric Acid Content of Animal Tissues, with Reference to Its Occurrence in Bone and Tumour. *Biochem. J.* **1941**, *35* (8–9), 1011–1023.

(26)   Reid, D. G.; Duer, M. J.; Jackson, G. E.; Murray, R. C.; Rodgers, A. L.; Shanahan, C. M. Citrate Occurs Widely in Healthy and Pathological Apatitic Biomineral: Mineralized Articular Cartilage, and Intimal Atherosclerotic Plaque and Apatitic Kidney Stones. *Calcif. Tissue Int.* **2013**, *93* (3), 253–260.

(27)   Schwarcz, H. P.; Agur, K.; Jantz, L. M. A New Method for Determination of Postmortem Interval: Citrate Content of Bone. *J. Forensic Sci.* **2010**, *55* (6), 1516–1522.

(28)   Jiang, W.; Chu, X.; Wang, B.; Pan, H.; Xu, X.; Tang, R. Biomimetically Triggered Inorganic Crystal Transformation by Biomolecules: A New Understanding of Biomineralization. *J. Phys. Chem. B* **2009**, *113* (31), 10838–10844.

(29)    Hu, Y. Y.; Rawal, A.; Schmidt-Rohr, K. Strongly Bound Citrate Stabilizes the Apatite Nanocrystals in Bone. *Proc. Natl. Acad. Sci.* **2010**, *107* (52), 22425–22429.

(30)    Xie, B.; Nancollas, G. H. How to Control the Size and Morphology of Apatite Nanocrystals in Bone. *Proc. Natl. Acad. Sci.* **2010**, *107* (52), 22369–22370.

(31)    Davies, E.; Müller, K. H.; Wong, W. C.; Pickard, C. J.; Reid, D. G.; Skepper, J. N.; Duer, M. J. Citrate Bridges between Mineral Platelets in Bone. *Proc. Natl. Acad. Sci.* **2014**, *111* (14), E1354-E1363.

(32)    Degli Esposti, L.; Adamiano, A.; Tampieri, A.; Ramirez-Rodriguez, G. B.; Siliqi, D.; Giannini, C.; Ivanchenko, P.; Martra, G.; Lin, F. H.; Delgado-López, J. M.; et al. Combined Effect of Citrate and Fluoride Ions on Hydroxyapatite Nanoparticles. *Cryst. Growth Des.* **2020**, *20* (5), 3163–3172.

(33)    Santos, C.; Almeida, M. M.; Costa, M. E. Morphological Evolution of Hydroxyapatite Particles in the Presence of Different Citrate:Calcium Ratios. *Cryst. Growth Des.* **2015**, *15* (9), 4417–4426.

(34)    Shao, C.; Zhao, R.; Jiang, S.; Yao, S.; Wu, Z.; Jin, B.; Yang, Y.; Pan, H.; Tang, R. Citrate Improves Collagen Mineralization via Interface Wetting: A Physicochemical Understanding of Biomineralization Control. *Adv. Mater.* **2018**, *30* (8), 1–7.

(35)    Saxena, N.; Habelitz, S.; Marshall, G. W.; Gower, L. B. Remineralization of Demineralized Dentin Using a Dual Analog System. *Orthod. Craniofac. Res.* **2019**, *22* (S1), 76–81.

(36)    Nassif, N.; Martineau, F.; Syzgantseva, O.; Gobeaux, F.; Willinger, M.; Coradin, T.;

Cassaignon, S.; Azaïs, T.; Giraud-Guille, M. M. In Vivo Inspired Conditions to Synthesize Biomimetic Hydroxyapatite. *Chem. Mater.* **2010**, *22* (12), 3653–3663.

(37)     Robin, M.; Euw, S. Von; Renaudin, G.; Gomes, S.; Krafft, J.; Nassif, N.; Costentin, G. Insights into OCP Identification and Quantification in the Context of Apatite Biomineralization. *CrystEngComm* **2020**, *22* (16), 2728-2742.

(38)     Somrani, S.; Banu, M.; Jemal, M.; Rey, C. Physico-Chemical and Thermochemical Studies of the Hydrolytic Conversion of Amorphous Tricalcium Phosphate into Apatite. *J. Solid State Chem.* **2005**, *178* (5), 1337–1348.

(39)     Giraud Guille, M. M.; Helary, C.; Vigier, S.; Nassif, N. Dense Fibrillar Collagen Matrices for Tissue Repair. *Soft Matter* **2010**, *6* (20), 4963.

(40)     Gobeaux, F.; Belamie, E.; Mosser, G.; Davidson, P.; Panine, P.; Giraud-Guille, M. M. Cooperative Ordering of Collagen Triple Helices in the Dense State. *Langmuir* **2007**, *23* (11), 6411–6417.

(41)     Helary, C.; Foucault-Bertaud, A.; Godeau, G.; Coulomb, B.; Giraud Guille, M. M. Fibroblast Populated Dense Collagen Matrices: Cell Migration, Cell Density and Metalloproteinases Expression. *Biomaterials* **2005**, *26* (13), 1533–1543.

(42)     Wang, Y.; Silvent, J.; Robin, M.; Babonneau, F.; Meddahi-Pellé, A.; Nassif, N.; Giraud Guille, M. M. Controlled Collagen Assembly to Build Dense Tissue-like Materials for Tissue Engineering. *Soft Matter* **2011**, *7* (20), 9659–9664.

(43)     Bergman, I.; Loxley, R. Two Improved and Simplified Methods for the Spectrophotometric

Determination of Hydroxyproline. *Anal. Chem.* **1963**, *35* (12), 1961–1965.

(44)     Chatzipanagis, K.; Iafisco, M.; Roncal-Herrero, T.; Bilton, M.; Tampieri, A.; Kröger, R.; Delgado-López, J. M. Crystallization of Citrate-Stabilized Amorphous Calcium Phosphate to Nanocrystalline Apatite: A Surface-Mediated Transformation. *CrystEngComm* **2016**, *18* (18), 3170–3173.

(45)     Iafisco, M.; Ramírez-Rodríguez, G. B.; Sakhno, Y.; Tampieri, A.; Martra, G.; Gómez-Morales, J.; Delgado-López, J. M. The Growth Mechanism of Apatite Nanocrystals Assisted by Citrate: Relevance to Bone Biomineralization. *CrystEngComm* **2015**, *17* (3), 507–511.

(46)     Wang, Y.; Von Euw, S.; Fernandes, F. M.; Cassaignon, S.; Selmane, M.; Laurent, G.; Pehau-Arnaudet, G.; Coelho, C.; Bonhomme-Coury, L.; Giraud-Guille, M. M.; et al. Water-Mediated Structuring of Bone Apatite. *Nat. Mater.* **2013**, *12* (12), 1144–1153.

(47)     Griffanti, G.; Nazhat, S. N. Dense Fibrillar Collagen-Based Hydrogels as Functional Osteoid-Mimicking Scaffolds. *Int. Mater. Rev.* **2020**, *65* (8), 502–521.

(48)     Robin, M.; Almeida, C.; Azaïs, T.; Haye, B.; Illoul, C.; Lesieur, J.; Giraud-Guille, M. M.; Nassif, N.; Hélary, C. Involvement of 3D Osteoblast Migration and Bone Apatite during in Vitro Early Osteocytogenesis. *Bone* **2016**, *88*, 146–156.

(49)     Kim, D.; Lee, B.; Thomopoulos, S.; Jun, Y.-S. In Situ Evaluation of Calcium Phosphate Nucleation Kinetics and Pathways during Intra- and Extrafibrillar Mineralization of Collagen Matrices. *Cryst. Growth Des.* **2016**, *16* (9), 5359–5366.

(50) Navrotsky, A. Energetic Clues to Pathways to Biomineralization: Precursors, Clusters, and Nanoparticles. *Proc. Natl. Acad. Sci.* **2004**, *101* (33), 12096–12101.

(51) Wang, L.; Nancollas, G. H. Calcium Orthophosphates: Crystallization and Dissolution. *Chem. Rev.* **2008**, *108* (11), 4628–4669.

(52) Romberg, R. W.; Werness, P. G.; Riggs, B. L.; Mann, K. G. Inhibition of Hydroxyapatite Crystal Growth by Bone-Specific and Other Calcium-Binding Proteins. *Biochemistry* **1986**, *25* (5), 1176–1180.

(53) Hunter, G. K.; Hauschka, P. V.; Poole, R. A.; Rosenberg, L. C.; Goldberg, H. A. Nucleation and Inhibition of Hydroxyapatite Formation by Mineralized Tissue Proteins. *Biochem. J.* **1996**, *317* (1), 59–64.

(54) Termine, J. D.; Posner, A. S. Infrared Analysis of Rat Bone: Age Dependency of Amorphous and Crystalline Mineral Fractions. *Science.* **1966**, *153* (3743), 1523–1525.

(55) Rey, C.; Combes, C.; Drouet, C.; Glimcher, M. J. Bone Mineral: Update on Chemical Composition and Structure. *Osteoporos. Int.* **2009**, *20* (6), 1013–1021.

(56) Boonrungsiman, S.; Gentleman, E.; Carzaniga, R.; Evans, N. D.; Mccomb, D. W. The Role of Intracellular Calcium Phosphate in Osteoblast-Mediated Bone Apatite Formation. *Proc. Natl. Acad. Sci.* **2012**, *109* (35), 14170-14175.

(57) Akiva, A.; Kerschnitzki, M.; Pinkas, I.; Wagermaier, W.; Yaniv, K.; Fratzl, P.; Addadi, L.; Weiner, S. Mineral Formation in the Larval Zebra Fi Sh Tail Bone Occurs via an Acidic Disordered Calcium Phosphate Phase. *J. Am. Chem. Soc.* **2016**, *138* (43), 14481–14487.

(58) Mahamid, J.; Aichmayer, B.; Shimoni, E.; Ziblat, R.; Li, C.; Siegel, S.; Paris, O.; Fratzl, P.; Weiner, S.; Addadi, L. Mapping Amorphous Calcium Phosphate Transformation into Crystalline Mineral from the Cell to the Bone in Zebrafish Fin Rays. *Proc. Natl. Acad. Sci.* **2010**, *107* (14), 6316–6321.

(59) Wang, X.; Yang, J.; Andrei, C. M.; Soleymani, L.; Grand, K. Biomineralization of Calcium Phosphate Revealed by in Situ Liquid-Phase Electron Microscopy. *Commun. Chem.* **2018**, *1* (1), 1-7.

(60) Degli Esposti, L.; Adamiano, A.; Siliqi, D.; Giannini, C.; Iafisco, M. The Effect of Chemical Structure of Carboxylate Molecules on Hydroxyapatite Nanoparticles. A Structural and Morphological Study. *Bioact. Mater.* **2021**, *6* (8), 2360–2371.

(61) Chen, Y.; Gu, W.; Pan, H.; Jiang, S.; Tang, R. Stabilizing Amorphous Calcium Phosphate Phase by Citrate Adsorption. *CrystEngComm* **2014**, *16* (10), 1864–1867.

(62) Vandecandelaere, N.; Rey, C.; Drouet, C. Biomimetic Apatite-Based Biomaterials: On the Critical Impact of Synthesis and Post-Synthesis Parameters. *J. Mater. Sci. Mater. Med.* **2012**, *23* (11), 2593–2606.

(63) Wu, Y.; Ackerman, J. L.; Kim, H. M.; Rey, C.; Barroug, A.; Glimcher, M. J. Nuclear Magnetic Resonance Spin-Spin Relaxation of the Crystals of Bone, Dental Enamel, and Synthetic Hydroxyapatites. *J. Bone Miner. Res.* **2002**, *17* (3), 472–480.

(64) Peytcheva, A.; Cölfen, H.; Schnablegger, H.; Antonietti, M. Calcium Phosphate Colloids with Hierarchical Structure Controlled by Polyaspartates. *Colloid Polym. Sci.* **2002**, *280* (3), 218–227.

(65) Ruiz-Agudo, E.; Burgos-Cara, A.; Ruiz-Agudo, C.; Ibañez-Velasco, A.; Cölfen, H.; Rodriguez-Navarro, C. A Non-Classical View on Calcium Oxalate Precipitation and the Role of Citrate. *Nat. Commun.* **2017**, *8* (1), 1-10.

(66) Hu, Y. Y.; Liu, X. P.; Ma, X.; Rawal, A.; Prozorov, T.; Akinc, M.; Mallapragada, S. K.; Schmidt-Rohr, K. Biomimetic Self-Assembling Copolymer-Hydroxyapatite Nanocomposites with the Nanocrystal Size Controlled by Citrate. *Chem. Mater.* **2011**, *23* (9), 2481–2490.

(67) Filgueiras, M. R. T.; Mkhonto, D.; de Leeuw, N. H. Computer Simulations of the Adsorption of Citric Acid at Hydroxyapatite Surfaces. *J. Cryst. Growth* **2006**, *294* (1), 60–68.

(68) De Leeuw, N. H.; Rabone, J. A. L. Molecular Dynamics Simulations of the Interaction of Citric Acid with the Hydroxyapatite (0001) and (0110) Surfaces in an Aqueous Environment. *CrystEngComm* **2007**, *9* (12), 1178–1186.

(69) Wu, Y. J.; Tsai, T. W. T.; Huang, S. J.; Mou, Y.; Lin, C. J.; Chan, J. C. C. Hydrogen Bond Formation between Citrate and Phosphate Ions in Spherulites of Fluorapatite. *Langmuir* **2013**, *29* (37), 11681–11686.

(70) Katz, E. P.; Li, S. T. Structure and Function of Bone Collagen Fibrils. *J. Mol. Biol.* **1973**, *80* (1), 1–15.

(71) Xu, Z.; Yang, Y.; Zhao, W.; Wang, Z.; Landis, W. J.; Cui, Q.; Sahai, N. Molecular Mechanisms for Intrafibrillar Collagen Mineralization in Skeletal Tissues. *Biomaterials* **2015**, *39*, 59–66.

(72)     Wang, Y.; Von Euw, S.; Laurent, G.; Crevant, C.; Bonhomme-Coury, L.; Giraud-Guille, M. M.; Babonneau, F.; Nassif, N.; Azaïs, T. Impact of Collagen Confinement vs. Ionic Substitutions on the Local Disorder in Bone and Biomimetic Apatites. *Mater. Horizons* **2014**, *1* (2), 224–231.

(73)     Toroian, D.; Joo, E. L.; Price, P. A. The Size Exclusion Characteristics of Type I Collagen: Implications for the Role of Noncollagenous Bone Constituents in Mineralization. *J. Biol. Chem.* **2007**, *282* (31), 22437–22447.

(74)     Price, P. A.; Toroian, D.; Lim, J. E. Mineralization by Inhibitor Exclusion. The Calcification of Collagen with Fetuin. *J. Biol. Chem.* **2009**, *284* (25), 17092–17101.

(75)     Zuckerman, J. M.; Assimos, D. G. Hypocitraturia: Pathophysiology and Medical Management. *Rev. Urol.* **2009**, *11* (3), 134–144.

(76)     Giachelli, C. M. Inducers and Inhibitors of Biomineralization: Lessons from Pathological Calcification. *Orthod. Craniofacial Res.* **2005**, *8* (4), 229–231.

(77)     Stetler-Stevenson, W. G.; Veis, A. Bovine Dentin Phosphophoryn: Calcium Ion Binding Properties of a High Molecular Weight Preparation. *Calcif. Tissue Int.* **1987**, *40* (2), 97–102.

(78)     Boskey, A. L.; Villarreal-Ramirez, E. Intrinsically Disordered Proteins and Biomineralization. *Matrix Biol.* **2016**, *52–54*, 43–59.

(79)     He, G.; George, A. Dentin Matrix Protein 1 Immobilized on Type I Collagen Fibrils Facilitates Apatite Deposition in Vitro. *J. Biol. Chem.* **2004**, *279* (12), 11649–11656.

(80) Boonrungsiman, S. The Role of Intracellular Calcium Phosphate in Osteoblast-Mediated Bone Apatite Formation. *Proc. Natl. Acad. Sci.* **2012**, *109* (35), 14170–14175.

(81) Nitiputri, K.; Ramasse, Q. M.; Autefage, H.; McGilvery, C. M.; Boonrungsiman, S.; Evans, N. D.; Stevens, M. M.; Porter, A. E. Nanoanalytical Electron Microscopy Reveals a Sequential Mineralization Process Involving Carbonate-Containing Amorphous Precursors. *ACS Nano* **2016**, *10* (7), 6826–6835.

(82) Fornasier, V. L. Osteoid: An Ultrastructural Study. *Hum. Pathol.* **1977**, *8* (3), 243–254.

(83) Tovani, C. B. ; Gloter, A.; Azaïs, T.; Selmane, M.; Ramos, A. P.; Nassif, N. Formation of Stable Strontium-Rich Amorphous Calcium Phosphate: Possible Effects on Bone Mineral. *Acta Biomater.* **2019**, *92*, 315–324.

(84) Geng, Z.; Cui, Z.; Li, Z.; Zhu, S.; Liang, Y.; Lu, W. W.; Yang, X. Synthesis, Characterization and the Formation Mechanism of Magnesium- and Strontium-Substituted Hydroxyapatite. *J. Mater. Chem. B* **2015**, *3* (18), 3738–3746.

(85) Kniep, R.; Simon, P.; Rosseeva, E. Structural Complexity of Hexagonal Prismatic Crystal Specimens of Fluorapatite-Gelatine Nanocomposites: A Case Study in Biomimetic Crystal Research. *Cryst. Res. Technol.* **2014**, *49* (1), 4–13.

(86) Silvent, J.; Robin, M.; Bussola Tovani, C.; Wang, Y.; Soncin, F.; Delgado, S.; Azaïs, T.; Sassoye, C.; Giraud-Guille, M.-M.; Sire, J.-Y.; et al. Collagen Suprafibrillar Confinement Drives the Activity of Acidic Calcium-Binding Polymers on Apatite Mineralization. *Biomacromolecules* **2021**, acs.biomac.1c00206.

(87)    Jiang, W.; Griffanti, G.; Tamimi, F.; McKee, M. D.; Nazhat, S. N. Multiscale Structural

Evolution of Citrate-Triggered Intrafibrillar and Interfibrillar Mineralization in Dense

Collagen Gels. *J. Struct. Biol.* **2020**, *212* (1), 107592.

(88)    Glimcher, M. J. Bone: Nature of the Calcium Phosphate Crystals and Cellular, Structural,

and Physical Chemical Mechanisms in Their Formation. *Rev. Mineral. Geochemistry* **2006**,

*64* (1), 223–282.

# The concentration of bone-related organic additives drives the pathway of apatite formation

*Marc Robin[1§], Camila B. Tovani[1§], Jean-Marc Krafft[2], Guylène Costentin[2]\*, Thierry Azaïs[1], Nadine Nassif[1]\**

TOC graphic
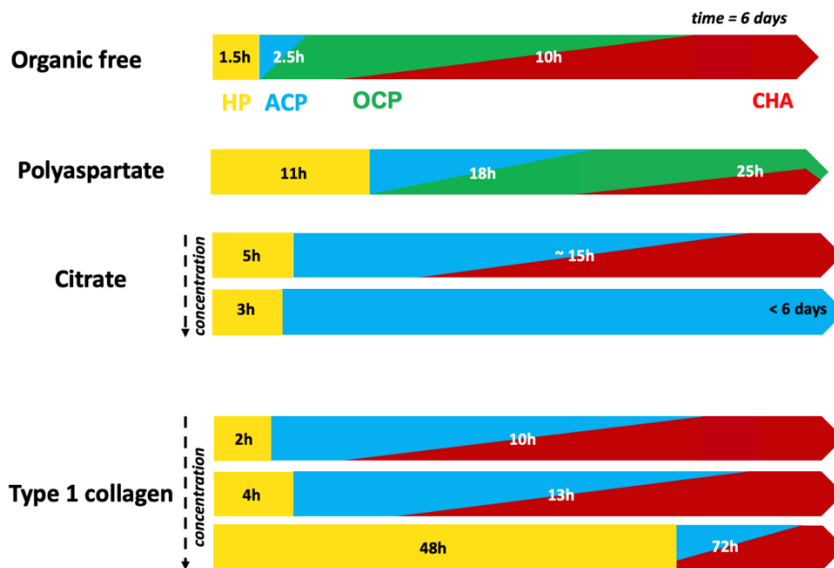


Synopsis

By playing with the concentration of bone organic additives, the work helps to identify their specific effects on apatite formation.

**The concentration of bone-related organic additives drives the pathway of apatite formation**

Marc Robin[1][§], Camila Bussola Tovani[1][§], Jean-Marc Krafft[2], Guylène Costentin[2],\* Thierry Azaïs[1], Nadine Nassif[1]\*

1. Sorbonne Université, CNRS, Collège de France, Laboratoire Chimie de la Matière Condensée de Paris, LCMCP, F-75005 Paris, France.

2. Sorbonne Université, CNRS, Laboratoire Réactivité de Surface, LRS, F-75005 Paris, France.

[§] These authors contributed equally to this work

\*Corresponding author. E-mail:

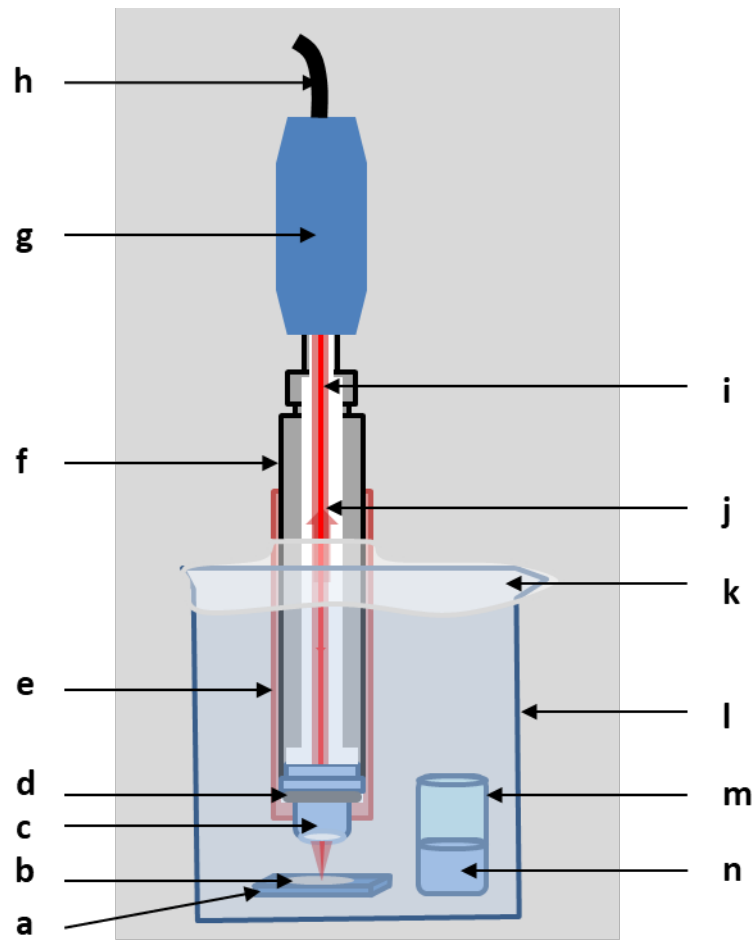guylene.costentin@sorbonne-universite.fr, nadine.nassif@sorbonne-universite.fr

**Fig. S1** Schematic representation of the homemade *in situ* Raman set up developped for the CaP formation in the presence of collagen: an aluminum tube with threaded ends carrying a 10x lens and wrapped with PTFE was screwed to the optical head.

a: quartz plate; b: sample; c; microscope lens 10x; d: O ring; e: cylindrical shell in PTFE; f: aluminum tube; g: Raman MR-Probe (Kaiser Optical Systems); h: optical fibers; i: laser beam; j: collected Raman signal; k: parafilm; l: 1L beaker; m: flask; n: $NH_3$
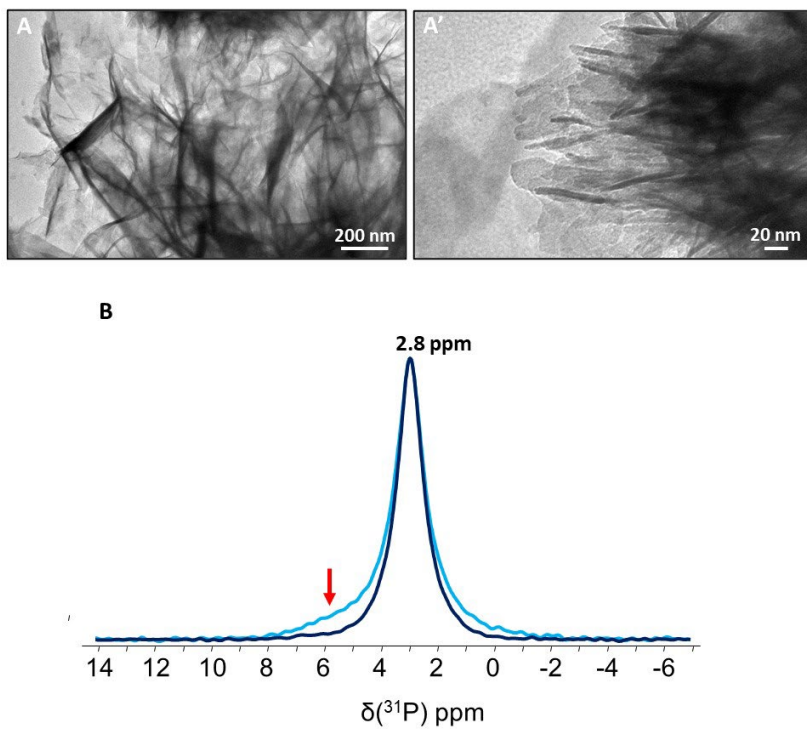
**Fig. S2** (A-A') TEM images of biomimetic apatite (CHA) and (B) $^{31}$P ss NMR spectra
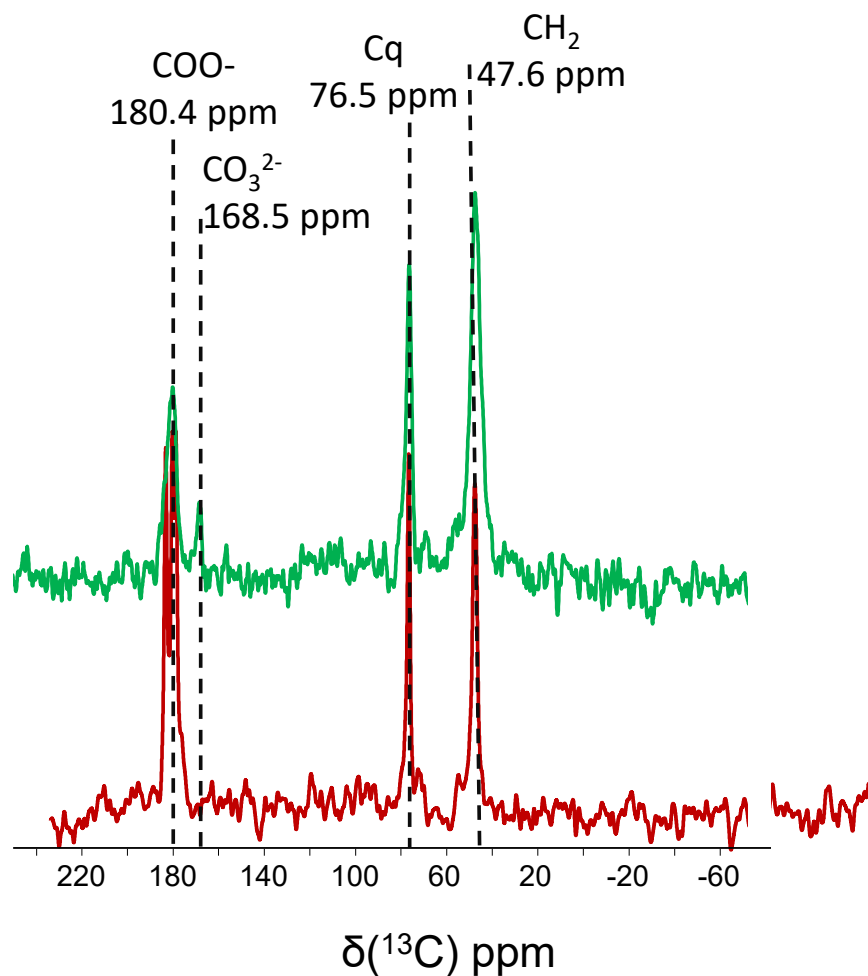
**Fig. S3** Comparison of the $^1$H-$^{13}$C CP MAS ssNMR spectra ($t_{CP}$ = 1 ms) of ACP-cit2% (green line) and crystallized citrate (red line). Resonance peaks from citrate are observed at $\delta(^{13}$C) = 180.4, 76.5 and 47.6 ppm; they are assigned to carboxylic group, quaternary carbon (Cq) and CH$_2$ groups, respectively. The resonance at $\delta(^{13}$C) = 168.5 ppm is due to inorganic carbonate.
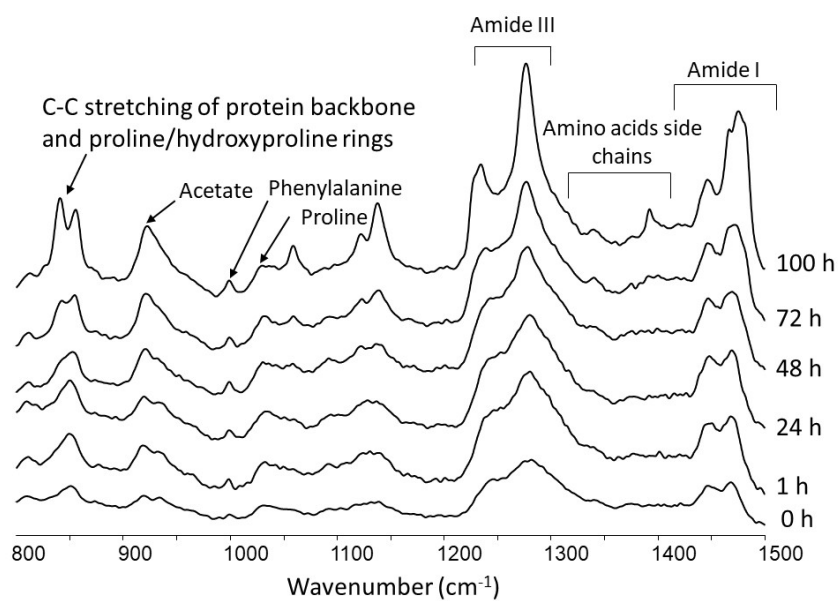
**Fig. S4** Raman spectra acquired at different reaction time for 250 mg mL$^{-1}$ collagen matrix containing the ionic precursors.